# Particle size segregation in a two-dimensional bed undergoing vertical vibration

W. Cooke,[1] S. Warr,[1] J. M. Huntley,[2] and R. C. Ball[1]
[1]*Cavendish Laboratory, University of Cambridge, Madingley Road, Cambridge CB3 0HE, United Kingdom*
[2]*Department of Mechanical Engineering, Loughborough University of Technology, Loughborough LE11 3TU, United Kingdom*
(Received 27 June 1995; revised manuscript received 20 September 1995)

We present experimental results on the size-ratio and acceleration dependences of particle size segregation behavior for a single intruder in a two-dimensional bed of monodisperse particles undergoing vertical vibration at low accelerations. Using trajectory maps based on digital high speed photography and computer image processing we find that, at all base accelerations, the intruder and surrounding particles move upwards at the same speed. The motor of such convective motion is slip planes and block motion of particles slipping past each other which push the intruder and surrounding particles upwards in a collective motion. Although some of these features have been previously observed, we use these observations to propose a mechanism for segregation at low accelerations. In this the intermittent steplike motion is found to be due to the finite frequency of slip planes and dislocations, causing the intruder and surrounding particles to move upwards in finite-size jumps. The stability of the intruder is not relevant in our experiments and no fundamental difference in mechanism between the so-called intermittent and continuous regimes exists; only the frequency of slip planes and block motions is important.

PACS number(s): 46.10.+z, 47.27.Te, 64.75.+g

## I. INTRODUCTION

Granular materials are widely encountered in industry, generally in the form of mixtures of particles of various sizes. During the processing of these materials, for example, in pipe and hopper flow, mixing, and storage, particles with different characteristics separate out, or segregate [1,2]. This can cause major problems, particularly in the demixing of solid-solid mixtures [3]. Segregation can also occur through differences in particle density and shape, but size segregation is the most important effect [4]. Segregation is often driven by shaking, and it is this process that has received considerable attention in recent years.

A number of possible mechanisms for the segregation process has been presented in the literature, all having relevance in different regimes. In the low amplitude and high frequency regime, convection rolls, driven by particle-wall friction, control segregation [5]. At higher accelerations, explored using Monte Carlo computer simulation techniques [6–9], the convection rolls become unstable and the granular material becomes dilated with free volume introduced during each shaking cycle. The smaller particles fall relatively freely, while the intruders, requiring larger voids to fall downwards, are prevented from doing so by the statistical unlikelihood of collective motion forming such voids; the intruder therefore rises, or segregates. In this regime, segregation has been interpreted as the result of competition between independent-particle and collective reorganizations [10,11].

At the other extreme of low accelerations, recent experiments on two-dimensional systems have identified a transition from a continuous to intermittent motion as the particle size decreases [12,13]. At relatively large accelerations, global convection rolls are seen to carry the intruder at the same velocity [12], leading to the continuous ascent. In the low amplitude, low acceleration regime [13], experiments have indicated that segregation is no longer driven by convection, and intermittent, steplike motion is observed. The intermittent regime is accompanied by density microfluctuations [13], which clearly play a role in the segregation process. Under these conditions, an arching effect model has been proposed [14] to explain the continuous-intermittent transition. A Monte Carlo algorithm has recently been used by Dippel and Luding [15] to investigate these geometrical effects when convection is absent. A triangular hole was observed below the intruder, which leads to stability criterion for the intruder, which is again used to explain the continuous and intermittent regimes.

Deterministic, ordered sequential algorithms [16–18] predict a critical size ratio below which segregation does not occur [16,17]. This provoked controversy [19–22], but the critical size ratio has been identified with the continuous-intermittent transition rather than with a segregation threshold [13,20]; the simple deterministic model also exhibits both regimes when noise is included in the algorithm.

In this paper we present experimental results on the effect of size ratio, acceleration, and intruder start depth on the rise characteristics. In contrast to previous results, we find that convection rolls drive the segregation process in both the continuous and intermittent regimes. The intermittent motion is due to the finite frequency of dislocations (where two close packed regions slip past each other) and block motions in the matrix of background particles that are associated with convection and heaping at very low accelerations and over very long time scales.

 

## II. EXPERIMENTAL METHOD

The segregation cell consists of two glass plates (200 by 250 $mm^2$) mounted in an aluminum frame that allows the plate-plate separation to be adjusted by spacers of varying thickness. Approximately 5000 oxidized Duralumin, 2-mm-diam spheres form a monolayer between the glass plates, the spacing being adjusted to be fractionally greater than the spheres' diameter. A set of intruders consists of 1-mm thick Duralumin disks of various diameters, through which three 2-mm-diam chrome steel spheres are pressed, forming an equilateral triangle. This method for ensuring stability of the intruder was first introduced by Duran *et al.* [13] and is shown in Fig. 1; these steel spheres ensure that the intruder remains vertical. In the experiments, we used seven different sizes of intruders, 6, 10, 14, 18, 22, 26, and 30 mm in diameter, and their edges were lightly roughened with emery paper to standardize the sphere-intruder friction.

The cell was mounted on an electromagnetic shaker driven by a low distortion sinusoidal signal generator and a 1-kW power amplifier. Vertical accelerations were measured using a pair of piezoelectric accelerometers, mounted on either side of the cell. The cell was illuminated from the rear using a stabilized halogen light source and a plastic fresnel field lens. A Kodak Ektapro 1000 digital high speed camera was used to film the particle motion. At a resolution of 239 by 192 pixels, recording at 1000 frames per second gave a total recording time of 1.6 s. Longer time scales are achieved by synchronizing the camera with the logic pulse from the signal generator and recording a single frame at a constant phase. Passing the logic pulse through a divide by $n$ circuit allowed one frame to be recorded every $n$ cycles so that experiments lasting for up to 4 h, in real time, can be analyzed. The digital frames were downloaded to a Sun IPX SPARCstation computer for image processing. Particle centers are determined using the Hough transform technique [23], which has been further developed to analyze systems with several particle sizes [24]. Figure 2 shows an example bitmap of the intruder and background particles after the Hough transform has been applied. Circles drawn around the particles indicate that their centers have been located. Particle tracking software is then used to follow the motion of the intruder disk, and at higher magnifications the background particles can also be tracked through the frames.

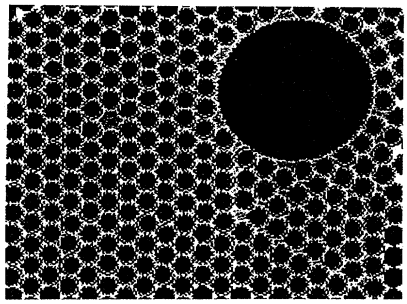

FIG. 2. Bit map showing the detection of particle centers, based on the use of Hough transforms, when two different sizes are present. Circles are drawn around detected particles.

The experiments were performed using a sinusoidal excitation of the form $y(t)=A_0\sin\omega t$, where $A_0$ is the amplitude and $\omega$ the angular frequency of the excitation. Experiments reported here were carried out at 10 Hz, and all accelerations are expressed by the reduced acceleration parameter $\Gamma=A_0\omega^2/g$. Further experiments were also performed using a laboratory-built programmable signal generator, which supplies a random displacement to the shaker (i.e., Gaussian velocity distribution function for the base). The root mean square base acceleration was used to characterize this system.

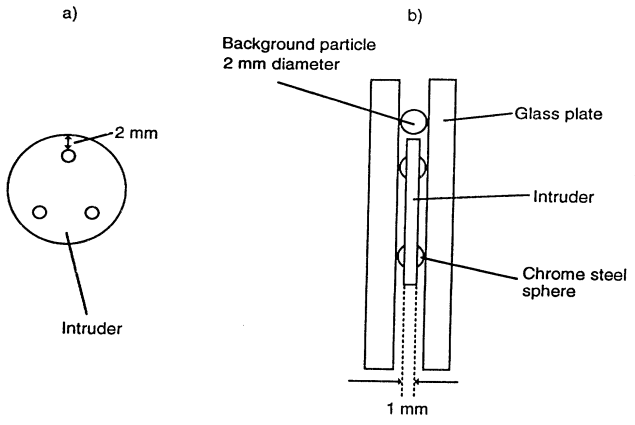


FIG. 1. (a) Front view of intruder disk showing the three chrome steel spheres inserted for stability. (b) Side view of intruder between the glass walls. The wall spacing is fractionally greater than the sphere's diameter. The method follows that initially proposed by Duran *et al.* [13].

## III. RESULTS AND DISCUSSION

In the experiments reported, the intruder was centered midway between the walls near the base of the cell with the background matrix of particles initially about 120 mm deep, thus avoiding surface wave phenomena. (In all cases the intruder start position was below the field of view of the camera, and the background matrix was initially in a disordered state above the intruder and ordered below.) The effect of the size ratio $\Phi=R/r$, where $R$ and $r$ are the intruder and background particle radii, respectively, on the rise characteristics is shown in Fig. 3 for $\Gamma$ in the range 1.33–1.34, corresponding to $A_0$ between 3.3 and 3.33 mm. The intruder was located midway between the segregation cell walls for each experiment. The intruder center was determined at constant phase, once per cycle, and filming started when each intruder was clearly visible in the camera field of view (thus trajectories are rescaled to a common origin). Figure 3 shows that the rise velocity increases with intruder radius and shows

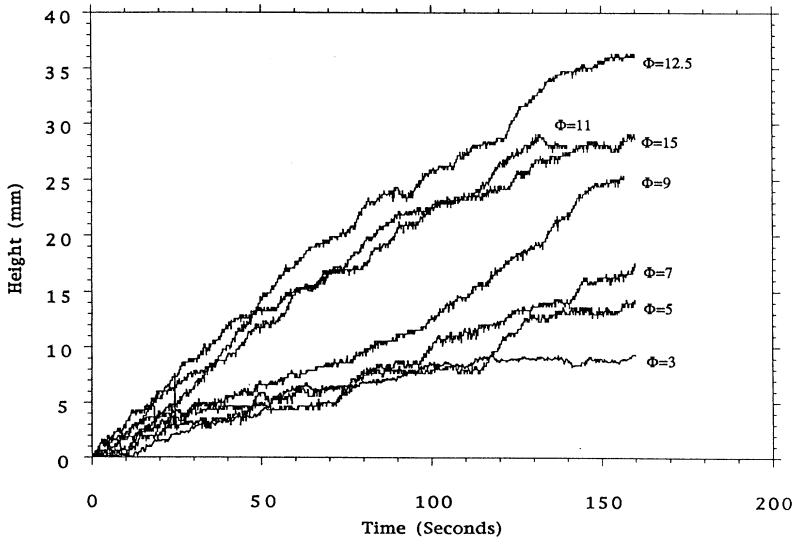


FIG. 3. Intruder height in pixels plotted against time for a range of size ratios $\Phi=3$, 5, 7, 9, 11, 12.5, and 15. The motion was filmed at one frame per cycle.

signs of the intermittent regime at small sizes. The initial intruder depth was not constant in these early results, and the result for the 30-mm-diam intruder gave a slower rise rate than expected, based on the trend shown by the other intruder sizes.

We therefore investigated the effect of initial intruder depth. In Fig. 4 the initial start depths of the 14-mm-diam intruder, from the intruder top to the surface, over the range 70 to 100 mm were considered for $\Gamma=1.41$, corresponding to an $A_0$ to 3.5 mm. With this smaller intruder the rise rate increases as the starting depth increases, but beyond a certain depth the segregation effect is suppressed. In all subsequent experiments an initial start depth of around 95 mm was used. Figure 5 shows the effect of initial depth of the 30-mm-diam intruder. Comparing the trajectory pairs (i) and (iii) together with (ii) and (iv) (see figure caption for details) shows that the particle rise rate decreases as the initial start depth increases from 60 to 70 mm, so the point of suppression may be higher for larger intruders. These pairs also indicate that slight variations in the acceleration do not significantly change the behavior at a given start depth. Curiously, (v) indicates that a trajectory appears to remember its initial state. Such dependence of segregation rate on initial position has also been recently observed in computer simulations [25]. The strength of this height dependence as a function of intruder diameter is not clear at present. Some discussion about possible interpretations for the height dependence is given later in this paper, but there is still uncertainty about why this behavior occurs.

Considering the effect of peak reduced acceleration, Figs. 6–8 show rise profiles for the 6-, 14-, and 22-mm-diam intruders, respectively, over the total range $1.24 \leq \Gamma \leq 1.72$. Figure 9 further shows a profile at a very low acceleration level of $\Gamma=1.17$ for the 14-mm in-

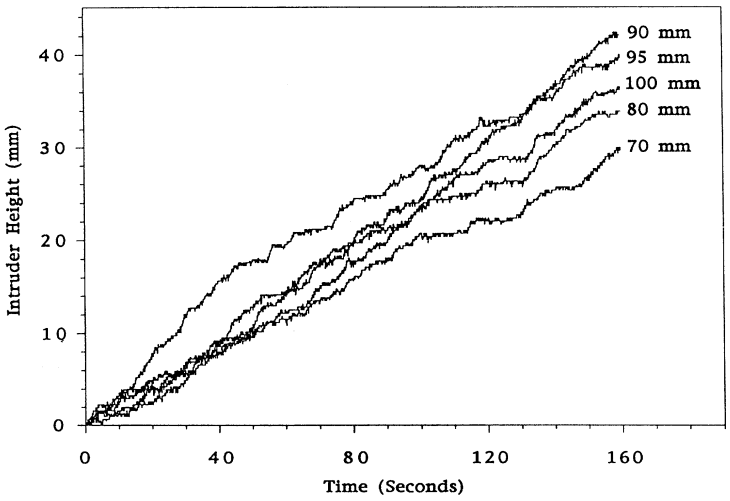


FIG. 4. Effect of initial intruder depth below the surface (measured to the top of the intruder) for a 14-mm-diam intruder vibrated at $\Gamma=1.4$. The height of the intruder center above the bottom of the camera field of view is plotted against time.

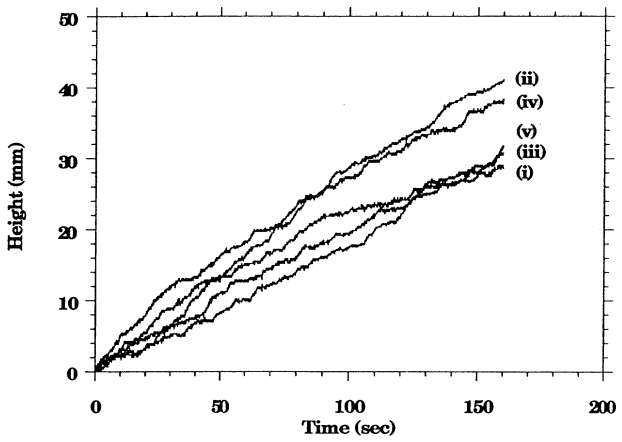


FIG. 5. Effect of initial intruder depth (measured to the top of the intruder) below the surface on the rise profile. (i) $\Gamma = 1.33 \pm 0.01$, start depth = 70 mm; (ii) $\Gamma = 1.28 \pm 0.01$, start depth = 60 mm; (iii) $\Gamma = 1.32 \pm 0.01$, start depth = 70 mm; (iv) $\Gamma = 1.37 \pm 0.01$, start depth = 60 mm; (v) $\Gamma = 1.35 \pm 0.01$, start depth = 75 mm. When the intruder reached 60 mm below the surface, the excitation was stopped, the surface was leveled, and the vibration then continued. In all cases the camera position was fixed, and filming took place when the intruder entered the field of view and the intruder height relative to the bottom of the field of view was plotted against time. One frame per cycle was taken.

truder where the particle centers were located once every 48 cycles (approximately 2 h in real time). The intermittent, steplike motion is clearly visible in Fig. 9 but less so at the higher $\Gamma$ values in the previous figures. Highly linear rise profiles are seen as $\Gamma$ increases, with some trajectories still showing significant fluctuations around this linear rise. The rise rate increases as $\Gamma$ increases, and Fig. 10 shows the average rise velocity as a function of $\Gamma$ for the three intruder diameters. Velocities were estimated by the slope of the best fit line through the trajectories, and the error bars indicate the uncertainty in the reduced accelerations values. As previously reported [13], we find a linear dependence of rise velocity with $\Gamma$ that extends over a wider range of intruder sizes.

Shortly we will consider the segregation mechanism, but first we want to consider the effect of the input shaker characteristics. To do this, we consider rise profiles with a random rather than a sinusoidal excitation. Figures 11 and 12 show the results for the lower and higher acceleration ranges, respectively; the root mean square base acceleration and initial start depth are shown on the figures. The motion was again filmed at one frame per cycle (of the random shake), and because the phase is not constant at this point the profiles take on a spiky appearance. The rise rate tends to increase with rms value of $\Gamma$, but no clear trends emerge. Qualitative observations showed that the same segregation mechanism occurs with the random and sinusoidal excitations. We subsequently confine our observations to those experiments using sinusoidal excitation because the constant phase enables detailed trajectory maps of the motion to be made.

Initially, to make sense of the above observations, we have analyzed the recorded frames from the experiment by snapshots of the particle motion and trajectory maps. When frames are recorded once every $n$ cycles, the segregation mechanism becomes clear, especially at low acceleration levels. Filming continuously at 1000 frames per second, for example, as shown in Fig. 13, where a 6-mm-diam intruder was vibrated at 50 Hz with a peak acceleration of $10g$, reveals an important detail. The particle oscillates up and down with the driving frequency and multiplies with a gentle linear rise superimposed on the motion. Over short time scales, of a few seconds, the intruder simply moves up and down with the background matrix of particles (especially at low $\Gamma$ values) and the segregation mechanism cannot be properly observed.

Over time scales 100 times longer, observation of images filmed once every cycle shows slip plane events, where two close packed blocks or regions of particles slip

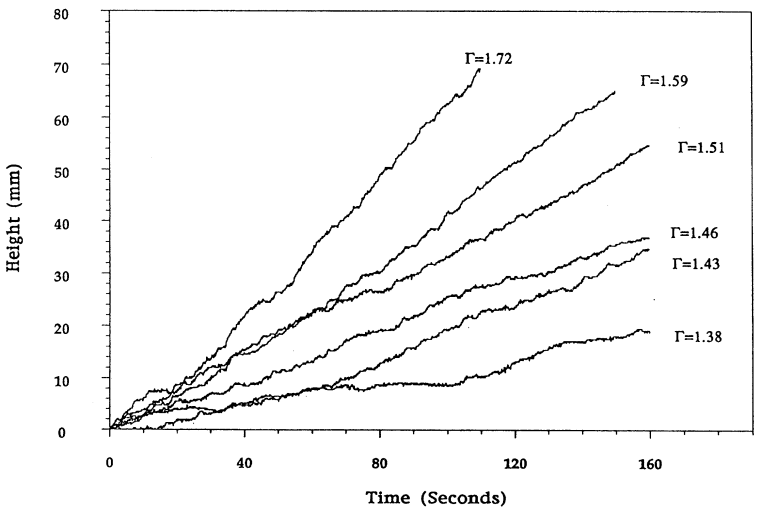


FIG. 6. Intruder height in millimeters plotted against time for a range of reduced accelerations, $\Gamma = 1.72$, 1.59, 1.51, 1.46, 1.43, and 1.38. These plots are at a constant size ratio $\Phi = 3$. The motion was filmed at one frame per cycle.

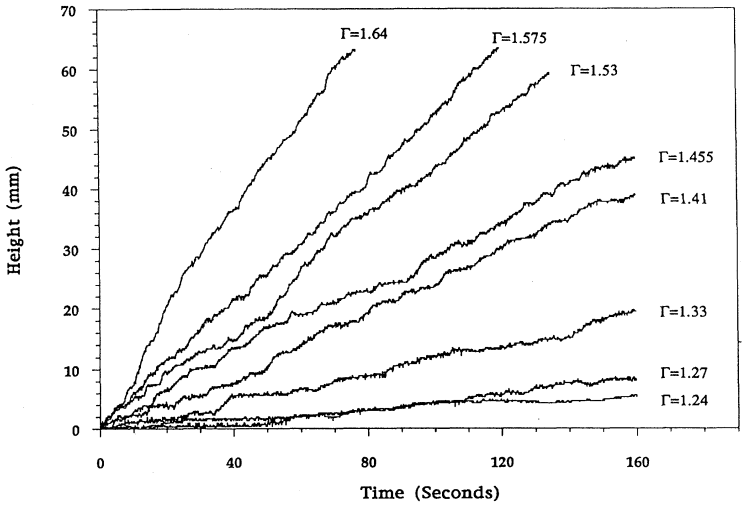


FIG. 7. Intruder height in millimeters plotted against time for a range of reduced accelerations, $\Gamma = 1.64$, 1.575, 1.53, 1.455, 1.41, 1.33, 1.27, and 1.24. These plots are at a constant size ratio $\Phi = 7$. The motion was filmed at one frame per cycle.

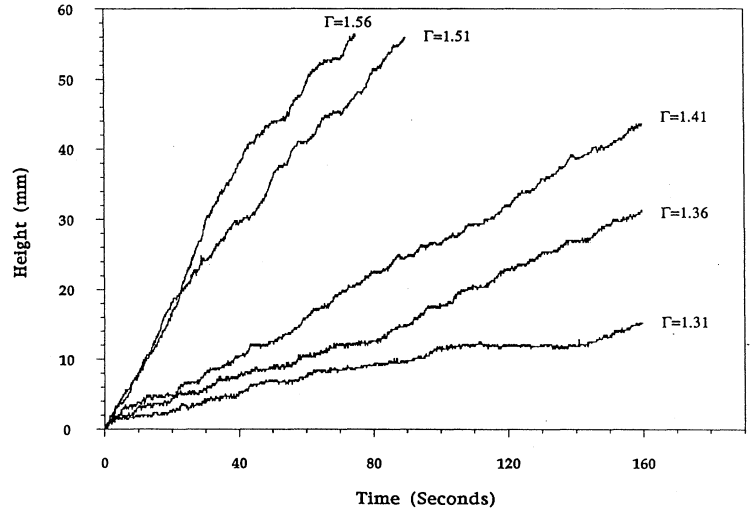


FIG. 8. Intruder height in millimeters plotted against time for a range of reduced accelerations, $\Gamma = 1.56$, 1.51, 1.41, 1.36, and 1.31. These plots are at a constant size ratio $\Phi = 12.5$. The motion was filmed at one frame per cycle.

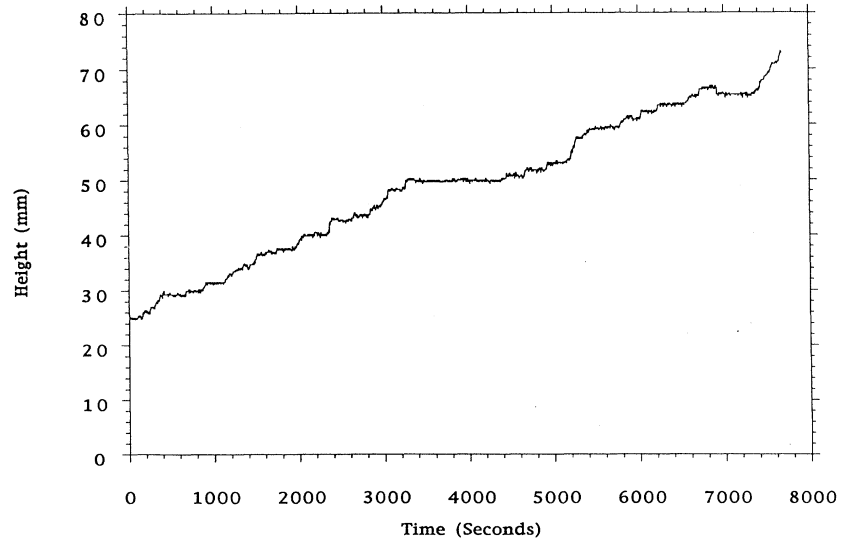


FIG. 9. Intruder height in pixels plotted against time for a low acceleration, $\Gamma = 1.17$, and size ratio $\Phi = 7$. The intermittent motion is clearly visible in this regime, which was filmed at one frame every 48 cycles.

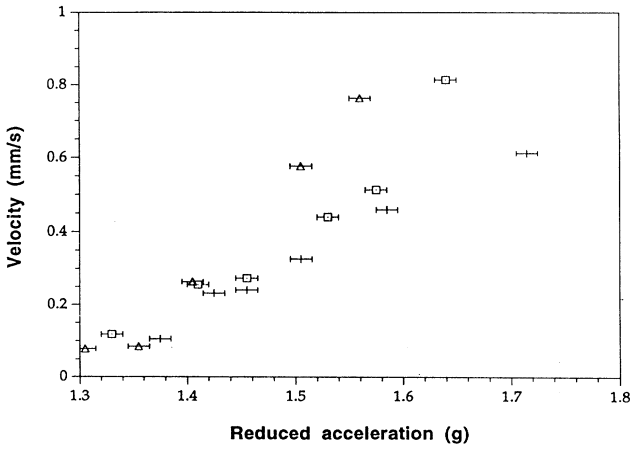


FIG. 10. Average rise velocity (from least-squares-fit line through the trajectories) against dimensionless acceleration. Crosses, squares, and triangles correspond to $\Phi=3$, 7, and 12.5, respectively. An approximately linear rise in average velocity is observed for each case.

past one another. These are intimately connected with the motion of the intruder at small $\Phi$ and low $\Gamma$ and provide the dominant mechanism for segregation. Previous experiments [12,13] reported observations of reversible cracks, which sometimes resulted in irreversible cracks such as horizontal slip lines. These microfluctuations and geometrical effects were considered to control segregation, and an arching effect model was then proposed to account for the low acceleration behavior. Because of differences between the experimental setups, we are uncertain about the precise correspondence between these two sets of observations. The main differences between these and previously reported experiments [13,14] are, in our case, a slightly larger particle size and larger overall cell size; Duralumin spheres are slightly harder than aluminum and therefore have a higher restitution coefficient; we made no attempt to arrange a regular lattice arrangement at the start of the experiment. However, we present a detailed account of our observations, which then leads to a radically alternative interpretation concerning the segregation mechanism operating at low accelerations. We also note that further extensive work is required to assess, in detail, the precise effect of the above experimental variables on segregation characteristics and mechanism.

Initially, a distinction needs to be made between block motion caused by motion of the intruder (this is required for any intruder motion at low accelerations) and block motion that causes the intruder motion. It is blocks of particles moving upwards, from below, that push the intruder, together with the surrounding particles, upwards in finite-size jumps. The origin of slip planes and block motion is unclear at present, but it appears to originate at the walls. Particles move downwards along the walls and some can be pushed inwards from the walls, because of the local geometry, which then result in blocks of particles moving upward below the intruder. This also occurs without the intruder, but its presence may well influence the ease with which such motion occurs. Further extensive work is required to analyze this behavior and quantify the frequency and orientation of such slip planes.

To quantify this further, Figs. 14 and 15 show trajectory maps that are plotted for the 14-mm intruder with $\Gamma$ values of 1.65 and 1.32, corresponding to $A_0$ values of 4.11 and 3.29 mm, respectively. These maps show the motion of the background particles relative to the intruder together with the motion of the center of the intruder disk (motion filmed at one per phase). Figures 14–16 have been rotated by 90° so that the intruder moves from left to right over time. A magnification of 0.152 mm per pixel (or around 92 pixels per intruder diameter) is needed to accurately locate the centers of the background particles. In Fig. 14 the intruder rises through the convection mechanism previously reported

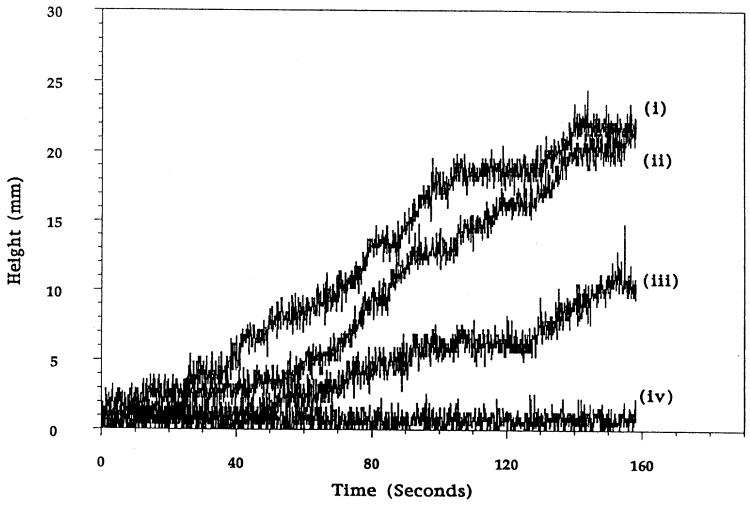


FIG. 11. Rise profiles obtained from a randomly shaken base rather than a sinusoidal excitation. An intruder with size rate $\Phi=7$ was used and the root-mean-square (rms) accelerations and initial start depths $h_0$ are as follows: (i) rms $=1.7-1.9g$; $h_0=93$ mm; (ii) rms $=1.6-1.8g$; $h_0=95$ mm; (iii) rms $=1.7-2.0g$; $h_0=95$ mm; (iv) rms $=1.5-1.7g$, $h_0=85$ mm.

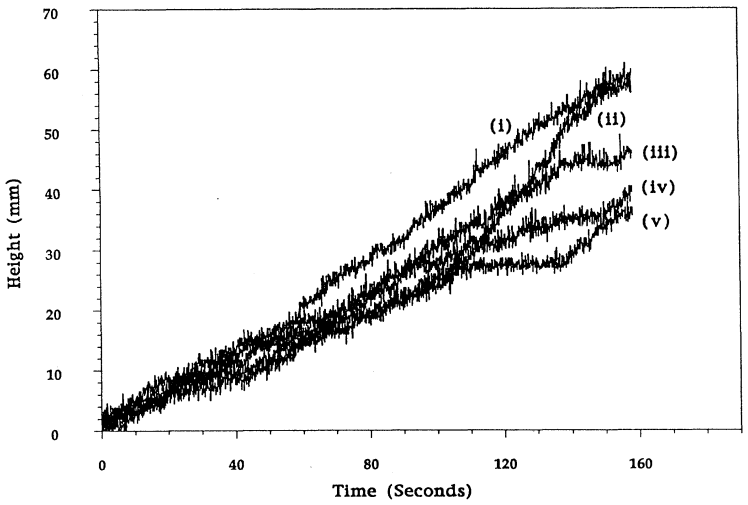


FIG. 12. Rise profiles obtained from a randomly shaken base rather than a sinusoidal excitation. An intruder with size ratio $\Phi=7$ was used and the root-mean-square (rms) accelerations and initial start depths $h_0$ are as follows: (i) rms$=1.9-2.2g$; $h_0=90$ mm; (ii) rms $=2.1-2.4g$; $h_0=95$ mm; (iii) rms$=2.0-2.3g$; $h_0=90$ mm; (iv) rms$=2.2-2.4g$, $h_0=95$ mm; (v) rms$=1.8-2.1g$; $h_0=95$ mm.

[5,13]. The intruder is carried upwards, at the same speed as the background particles, by the convective motion (defined to be consistent with previous work [13], i.e., that intruder and particles move upwards at the same speed), so that, relative to the intruder, they appear to fluctuate around an approximately constant location. Trajectory maps showing the global convection rolls have not been plotted because at the low magnifications required the background particles cannot be accurately tracked. The fluctuations from the lattice positions in Fig. 14 are due to the superposition of many local particle rearrangements and block motions, and it is this cooperative motion that causes the fluctuation in the intruder rise profile. Figure 15 shows a trajectory plot in the intermittent regime for a $\Gamma$ value of 1.32. This is around the lowest value at which significant motion occurs over the time scale of the experiment, but is not so low that filming needs to be done once every $n$ cycles ($n>1$). This map, however, does reflect the features that occur at much lower base accelerations, namely, that the fluctuation in the trajectories decreases and a more sharply defined crystalline arrangement results. Figure 15 indicates that both the intruder and background particles move upwards together at low accelerations. The local fluctuations in the traces are due to small scale particle reorganizations and block motion-slip planes. Such a block motion–slip plane event has been isolated in the trajectory map shown in Fig. 16. A total of 32 frames was used for this map, which was the time scale of the slip plane event. The block of particles moving upwards from below the intruder and at the same time pushing the intruder upwards are given by the regular array of dots on the right of the figure (recall that plots show motion relative to the intruder). The lines on the left therefore show particles falling away, relative to the intruder, and their curved nature indicates the dilatancy needed for such motion to occur.

Figures 17(a)–17(c) and 18(a)–18(c) show three

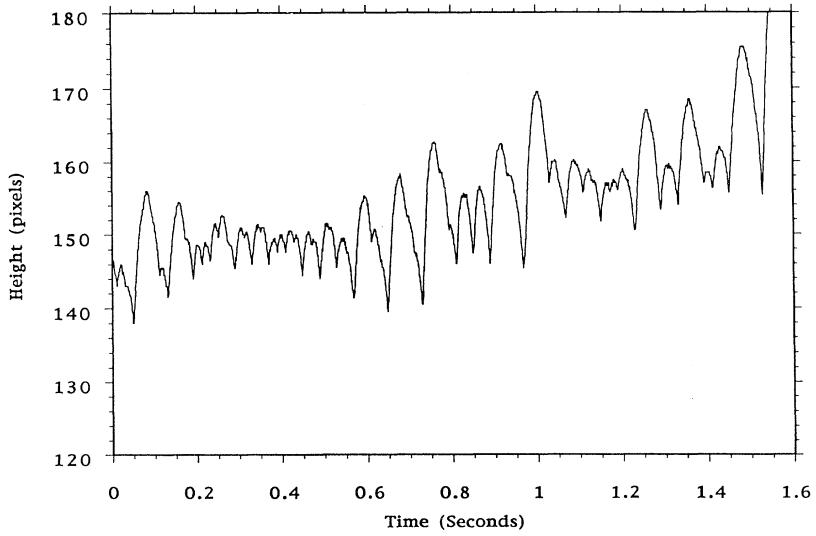


FIG. 13. Intruder height in pixels plotted against time for a 6-mm-diam intruder vibrated at 50 Hz and peak acceleration 10$g$. Filming continuously at 1000 frames per second shows the linear rise superimposed on the sinusoidal-like oscillations.

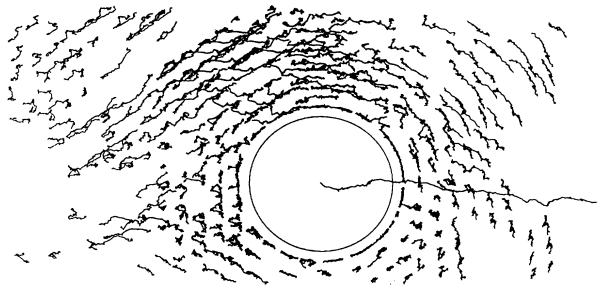

FIG. 14. Trajectory map showing the position of the background particles relative to the intruder disk. The intruder, with a size ratio $\Phi=7$, and its trajectory are also plotted. A reduced acceleration $\Gamma=1.65$ was used, so that we are in the regime of quite strong convection; the intruder moved over the field of view in 266 frames, which were used to generate this plot. The figure has been rotated by 90° so that the intruder moves from left to right across the page.

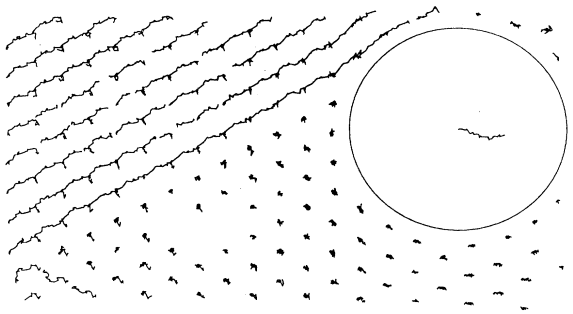

FIG. 16. Trajectory map showing the position of the background particles relative to the intruder disk. The intruder, with a size ratio, $\Phi=7$, and its trajectory are also plotted. A reduced acceleration $\Gamma=1.32$ was used so that we are in the regime with intermittent rise characteristics. 32 frames were used to generate this plot, which captures a single slip plane–block motion event. Dots indicate the moving block of particles, which push the intruder upwards, and the particles on the left therefore fall away relative to the intruder. The figure has been rotated by 90° so that the intruder moves from left to right across the page.

snapshots, each illustrating some of the features described above (the figures are rotated by 90 °, and the intruder therefore moves from left to right over time). Figure 17 shows the intruder and surrounding particles taken from the profile in Fig. 9, with a low acceleration of $\Gamma=1.17$, and Fig. 18 shows three snapshots from the profiles, with $\Gamma=1.65$ from Fig. 7. In Fig. 17 the overall packing density is high because the slip plane events occur relatively infrequently. In Fig. 17(a) one can see that the intruder disrupts the packing; the region immediately below the intruder can become disordered but soon orders when particles are pushed upwards or inwards from the sides. Slip planes can be angled, as shown in Fig. 17(b), where a block moves upward below the in-

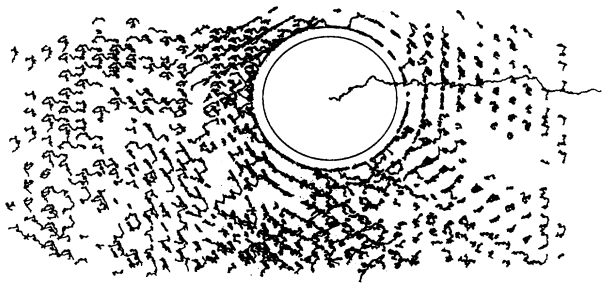

FIG. 15. Trajectory map showing the position of the background particles relative to the intruder disk. The intruder, with a size ratio $\Phi=7$, and its trajectory are also plotted. A reduced acceleration $\Gamma=1.32$ was used, so that we are in the regime with intermittent rise characteristics. The trajectories still resemble those of Fig. 14, showing that the intruder and background particles rise at the same rate in a collective motion; the intruder moved over the field of view in 1355 frames, which were used to generate this plot. The figure has been rotated by 90° so that the intruder moves from left to right across the page.

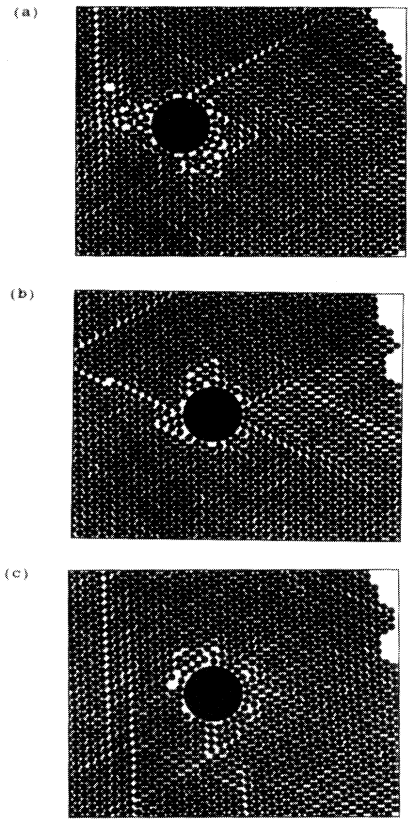


FIG. 17. Three snapshots of an intruder with size ratio $\Phi=7$, taken from the low acceleration ($\Gamma=1.17$), strongly intermittent profile shown in Fig. 9. These figures have been rotated by 90° so that the intruder moves from left to right across the page. (a) Regions of disorder often appear around the intruder. Small gaps may open up below the intruder, which particles can be pushed into by collective block motion; however, large gaps and avalanche events are not observed; (b) a slip plane is captured below the intruder, resulting in the upper block of particles moving upwards; (c) horizontal slip planes are often observed.

truder, or they often move horizontally, as shown in Fig. 17(c). Occasionally, a small gap opens up beneath the intruder and a layer or group of particles is pushed beneath the intruder through cooperative block motions. Avalanche events, where particles fall into a large gap below the intruder (see, for example, Ref. [15]), have not been observed. Generally, however, the same particles stay next to or close to the intruder as it moves upwards. At higher accelerations, these slip plane events are more frequent. In Fig. 18 the overall density is lower because the block slippages occur more frequently in this regime, where global convection rolls are observed, similar to those in the experiments of Duran *et al.* [13]. The three figures show snapshots from a block slippage event that occurs over a finite time and distance scale (Fig. 16 would be a sample trajectory map for such an event). Heaping is clearly seen, and nearly continual surface avalanches are found.

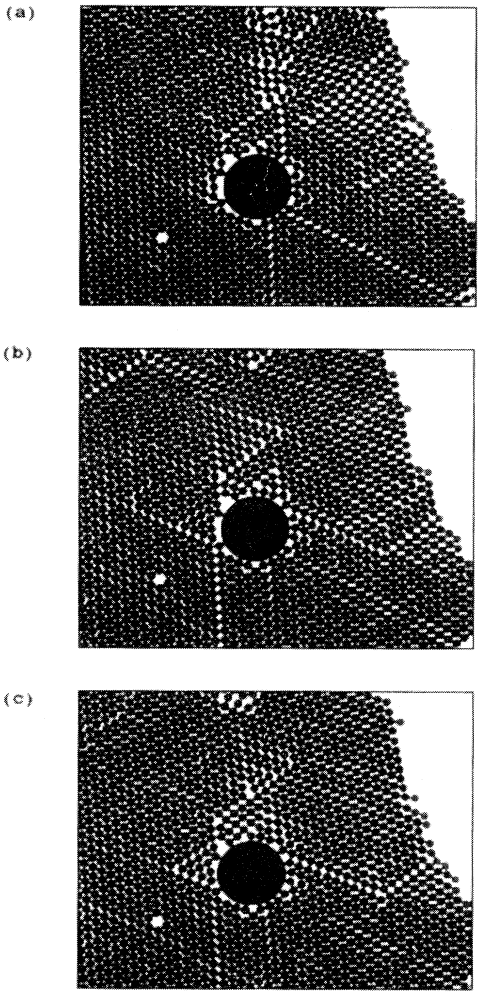


FIG. 18. Three snapshots of an intruder with size ratio $\Phi=7$, taken from the higher acceleration ($\Gamma=1.65$), linear, continuous rise profile shown in Fig. 7. These figures have been rotated by 90° so that the intruder moves from left to right across the page. Three stages of a slip plane event are shown, (a) at frame 517, (b) at frame 524, and (c) at frame 531, showing that the event takes a finite time to occur. It is this fact that allows detailed trajectory maps to be plotted.

At the lowest accelerations, symmetric heap formation is also observed, with occasional surface avalanches. At these low accelerations, previous two-dimensional experiments [26] found that convection rolls were initiated as small rolls at the walls in the upper corners. These rolls generate slip planes, and blocks of particles near the surface move upwards, generating the heap. We observe precisely this mechanism, which is an effect not seen in computer simulation studies [27–29]. Our new observation, however, is that whereas the small convection rolls dominate the heaping process, the block motion and slip planes constitute a cooperative motion, which even at the lowest accelerations pushes the intruder upwards at the *same speed* as the particles surrounding the intruder. Such a conclusion is clearly evident because the background particles in the trajectory maps stay in approximately the same positions relative to the intruder (which moves upwards by around two-particle diameters). Visual observation of the low $\Gamma$ images indicates that the frequency of such block motion is very low and such motion may constitute a convection roll on a much longer time scale and also have some part to play in the heaping mechanism. Further experimental work is required to determine precise trajectory maps in systems deemed to be undergoing convective motion. The effect of reducing the acceleration and including intruder particles on the trajectory map needs to be explored, and careful comparisons with plots from computer simulations need to be made.

Following the previous discussion, we therefore propose that the intermittent motion, at low $\Gamma$, is due to the finite frequency of these slip plane events and block motions pushing the intruder upwards. The intruder and background particles move upwards at the same speed, so that the intruder does not move through the particles "feeling" their local geometrical structure. A stable intruder appears to be present at all times so that the slip planes do not provide a driving force that pushes the intruder looking for stable positions; rather intruder jumps are related to the height a block of particles moves during a slip event. This is in contrast to other mechanisms that have been proposed for the origin of continuous and intermittent rise profiles [12–15]. Previous studies have concluded that convective motion is absent at low accelerations because the upwards motion of the intruder is not accompanied by upwards motion of the surrounding particles [13]. A geometrical arching effect model was, instead, initially proposed by Duran, Rajchenbach, and Clement [14] and analyzed by Monte Carlo simulation [15]. Figure 4 in Ref. [14] suggests that the intruder moves upwards relative to the smaller particles and searches for stable positions. In this interpretation, intermittent motion occurs with smaller intruders and large intruders move upwards continually. The intruder has to be pushed upwards by a fluctuation, with an unknown mechanism, and find a new stable position. Smaller intruders are less likely to be supported by an arch and

more likely to be held directly by the underlying array of spheres, thus making it more difficult to find a stable arch. This means that small intruders remain on a stable plateau until a fluctuation sufficient to get the particle onto the next plateau occurs. Such a geometrical arching effect would require that the intruder sample from a set of possible stable conditions. Such may be the case at higher accelerations, but in the regime studied here, where the intruder and background move largely as a collective, such sampling is not observed. The quality of the data is insufficient, at present, to analyze the statistics of the steps in the intermittent motion. When filming at one frame every 48 cycles, more than one slip event may occur between frames; however, we are currently trying to see if correlations between separate slip events exist.

Figures 19(a) and 19(b) show the power spectra for the velocity versus time profiles in the intermittent and continuous rise regimes, respectively. Here, we applied a forward difference operator

$$h'(t)=\frac{h(t+\Delta t)-h(t)}{\Delta t} \tag{1}$$

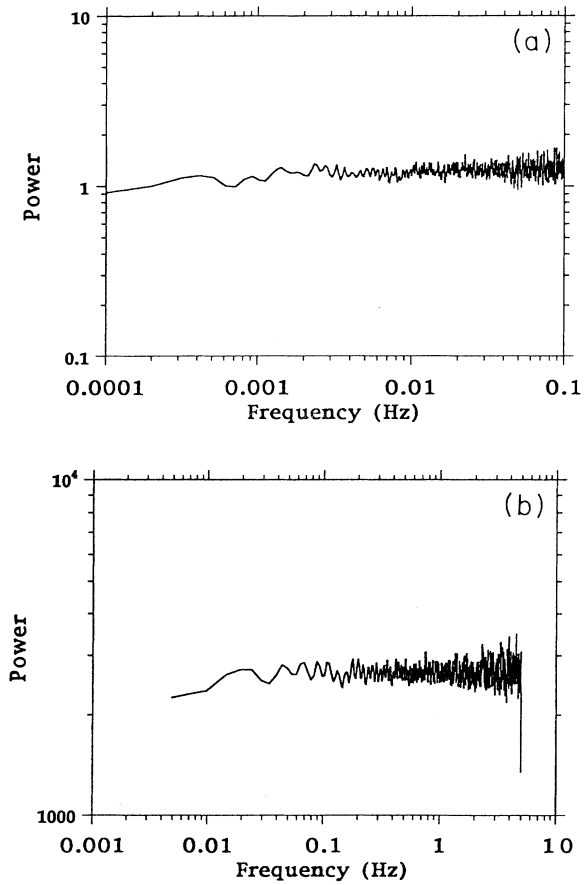


FIG. 19. Smoothed power spectra determined from the fast Fourier transform of height versus time data after a forward difference operator has been applied; (a) intermittent rise characteristics shown in Fig. 9; (b) continuous motion from Fig. 7 with $\Gamma=1.57$. The velocity power spectra show predominately white noise characteristics in both regimes.

to the height $h(t)$ versus time data, from Figs. 7 and 9, with $\Gamma=1.17$ and 1.57, respectively, before Fourier transforming. The spectra in the two regimes are remarkably similar, which indicates that the continuous rise profile shows intermittentlike characteristics in its fine structure. The power is dominated by random, uncorrelated events because predominantly white noise velocity power spectra are observed in both regimes. The transition between the two regimes may therefore be simply attributed to an increased frequency of block motions, which develop shorter, more randomly oriented dislocation boundaries, until the smooth streamlines in computer simulations [27–29] are seen at higher accelerations. These spectra therefore suggest that the distinction between continuous and intermittent rise may be rather arbitrary, with no fundamental difference in mechanism between the two regimes. As the acceleration increases, the surface convection rolls increase in size and strength [25] and influence the dislocation boundary breakdown at greater depths. The identification of a critical size ratio for a continuous-intermittent motion threshold thus has no physical significance.

With these observations in mind, the increase in rise rate with size ratio can be explained by the fact that a larger intruder results in a greater distortion of the regular lattice and a greater frequency of slip planes and block motions. The increase in rise rate with reduced peak acceleration, for a given side ratio, is due to the increased strength of convection rolls, also characterized by a greater frequency of slip planes and block motions. The reason for the variation with initial height is uncertain at present. Poschel and Herrmann [25] recently simulated the segregation and convection of 950 approximately 1-cm-diam disks at low frequencies (about 3 Hz) and high amplitudes ($A_0=2$ cm). At these higher amplitudes they find a critical frequency where the presence of the intruder triggers the onset of convection and then segregation. At this critical frequency, slightly lower initial placement of the intruder entirely suppresses the segregation effect. Experimentally, Knight *et al.* [30] found an exponential decay in the convection strength with depth. The computer simulations [25] show that at a critical frequency, the convection rolls extend deeper because of the presence of the intruder, which appears to pull the convection rolls downwards. These results suggest that the segregation is caused by the intruder being pulled up by the lower parts of the convection rolls. This is triggered at a critical frequency and is strongly dependent on the initial position of the intruder. We clearly observe an initial height dependence in our experiments, but this interpretation does not appear to be consistent with our observations in which the intruder is predominantly pushed upwards from below.

## IV. CONCLUSIONS

We have presented results on the segregation characteristics of a single intruder disk vertically vibrated in a two-dimensional array of background particles. At small size ratios and low peak accelerations, intermittent steplike motion is observed; and at larger size ratios and

higher accelerations, continuous and approximately linear rise profiles are observed. The segregation rate increases as the size ratio and peak acceleration increase.

We find, using trajectory maps, that the intruder disk rises at the same speed as the background particles over the entire range of accelerations studied. If we call such a phenomenon convective, then the mechanism of segregation is driven by convection rolls over all accelerations. Previous studies, which indicate that convection is absent at low accelerations (i.e., upwards motion of the intruder is not accompanied by upwards motion of the surrounding particles) and that geometrical effects strongly influence the segregation mechanism, are not supported by our observations. As in some previous studies [12,13], we find that motion of the background particles is characterized by slip planes and block motion of close packed particles moving past one another. We find that such motion pushes both the intruder and surrounding particles upwards in a collective motion, thus explaining the form of the trajectory maps. The intermittent motion at low accelerations is therefore due to the finite frequency of such slip planes and block motions that push the intruder upwards in a finite jump. The intruder is continually stable during this process and does not sample a configuration space of stable-unstable positions as it moves. Intensity spectra of continuous and intermittent rise profiles are similar and indicate no fundamental difference in mechanism between the two regimes As the acceleration increases, we conjecture that the frequency of slip planes and dislocations increases, so that intermittent motion becomes continuous. Further extensive work is needed to characterize and understand the origin of these slip planes and block motions and hence the exact nature and acceleration dependence of convection rolls. The relationship between the background particle motion and the jump characteristics at low accelerations needs to be explored further to check if stability criteria affect the behavior on a fine scale. Finally, we note that the effect of experimental variables, such as particle size, cell size, and small changes in restitution and friction coefficients, need to be determined.

## ACKNOWLEDGMENTS

This research was carried out as part of the Colloid Technology Collaborative Research Project with industrial sponsorship from Unilever Plc, ICI Plc, Zeneca Plc, Sclumberger Cambridge Research, and the Department of Trade and Industry. Dr. J. Duran, Professor S. F. Edwards, and Dr. C. C. Mounfield are thanked for fruitful discussions. C. Moss and G. T. H. Jacques are thanked for designing and constructing the programmable signal generator. Workshop support from R. Flaxmann and R. Halls is gratefully acknowledged.

[1] G. C. Barker, M. J. Grimson, and A. Mehta, in *Powders and Grains 93,* edited by C. Thorton (Balkema, Rotterdam, 1993), p. 253.
[2] G. C. Barker and M. J. Grimson, New Sci. **126**, May 26th, 37 (1990).
[3] H. Campbell and W. C. Bauer, Chem. Eng. **73** (3), 179 (1966).
[4] J. C. Williams, Powder Technol. **15**, 245 (1976).
[5] J. B. Knight, H. M. Jaeger, and S. R. Nagel, Phys. Rev. Lett. **70**, 3728 (1993).
[6] A. Rosato, F. Prinz, K. J. Standburg, and R. Swendsen, Powder Technol. **49**, 59 (1986).
[7] A. Rosato, K. J. Standburg, F. Prinz, and R. Swendsen, Phys. Rev. Lett. **58**, 1038 (1987).
[8] A. D. Rosato, Y. Lan, and D. T. Wang, Powder Technol. **66**, 149 (1991).
[9] A. Mehta and G. C. Barker, Phys. Rev. Lett. **67**, 394 (1991).
[10] G. C. Barker and A. Mehta, Nature (London) **364**, 486 (1993).
[11] A. Mehta and G. C. Barker, Rep. Prog. Phys. **57**, 383 (1994).
[12] J. Duran, T. Mazozi, J. Rajchenbach, and E. Clement, in *Soft Condensed Matter,* edited by K. K. Bardhan, B. K. Chakrabarti, and A. Hansen, Lecture Notes in Physics, Vol. 437 (Springer-Verlag, Berlin, 1994).
[13] J. Duran, T. Mazozi, E. Clement, and J. Rajchenbach, Phys. Rev. E **50**, 5138 (1994).
[14] J. Duran, J. Rajchenbach, and E. Clement, Phys. Rev. Lett. **70**, 2431 (1993).
[15] S. Dippel and S. Luding (unpublished).
[16] R. Jullien, P. Meakin, and A. Pavlovitch, Europhys. Lett. **22**, 523 (1993).
[17] R. Jullien, P. Meakin, and A. Pavlovitch, Phys. Rev. Lett. **69**, 640 (1992).
[18] R. Jullien and P. Meakin, Nature (London) **344**, 425 (1990).
[19] G. C. Barker, A. Mehta, and M. J. Grimson, Phys. Rev. Lett. **70**, 2194 (1993).
[20] R. Jullien, P. Meakin, and A. Pavlovitch, Phys. Rev. Lett. **70**, 2195 (1993).
[21] G. C. Barker and A. Mehta, Europhys. Lett. **29**, 61 (1995).
[22] R. Jullien, P. Meakin, and A. Pavlovitch, Europhys. Lett. **29**, 63 (1995).
[23] S. Warr, G. T. H. Jacques, and J. M. Huntley, Powder Technol. **81**, 41 (1994).
[24] G. T. H. Jacques (unpublished).
[25] T. Poschel and H. J. Herrmann, Europhys. Lett. **29**, 123 (1995).
[26] E. Clement, J. Duran, and J. Rajchenbach, Phys. Rev. Lett. **69**, 1189 (1992).
[27] Y-H. Taguchi, Phys. Rev. Lett. **69**, 1367 (1992).
[28] J. A. C. Gallas, H. J. Herrmann, and S. Sokolowski, Phys. Rev. Lett. **69**, 1371 (1992).
[29] S. Luding, E. Clement, and A. Blumen, Phys. Rev. E **50**, R1762 (1994).
[30] J. B. Knight, C. G. Fandrich, C. N. Lau, H. M. Jaeger, and S. R. Nagel (unpublished).

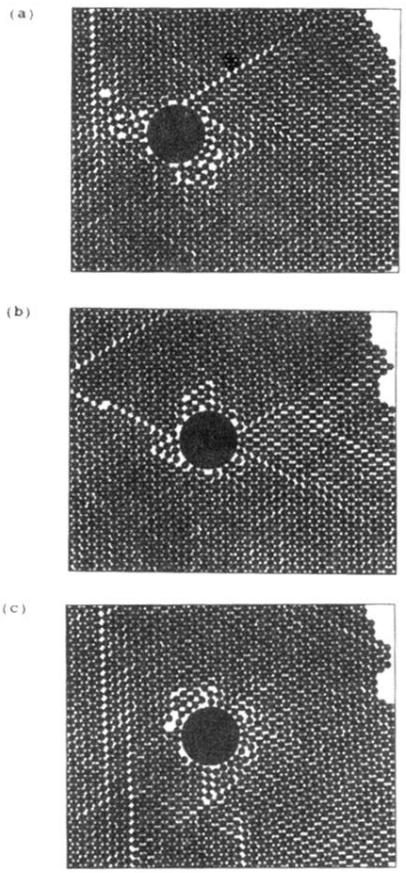


FIG. 17. Three snapshots of an intruder with size ratio $\Phi = 7$, taken from the low acceleration ($\Gamma = 1.17$), strongly intermittent profile shown in Fig. 9. These figures have been rotated by 90° so that the intruder moves from left to right across the page. (a) Regions of disorder often appear around the intruder. Small gaps may open up below the intruder, which particles can be pushed into by collective block motion; however, large gaps and avalanche events are not observed; (b) a slip plane is captured below the intruder, resulting in the upper block of particles moving upwards; (c) horizontal slip planes are often observed.

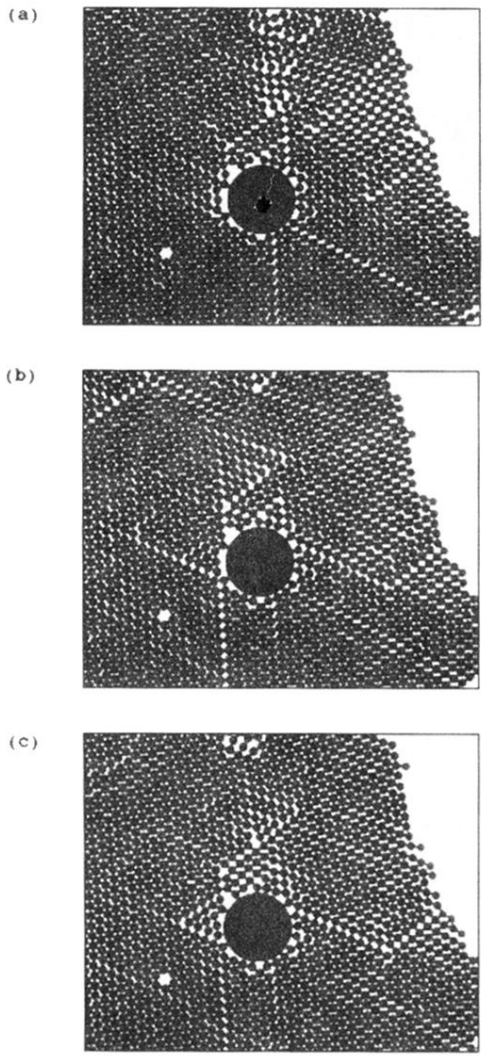


FIG. 18. Three snapshots of an intruder with size ratio $\Phi = 7$, taken from the higher acceleration ($\Gamma = 1.65$), linear, continuous rise profile shown in Fig. 7. These figures have been rotated by 90° so that the intruder moves from left to right across the page. Three stages of a slip plane event are shown, (a) at frame 517, (b) at frame 524, and (c) at frame 531, showing that the event takes a finite time to occur. It is this fact that allows detailed trajectory maps to be plotted.

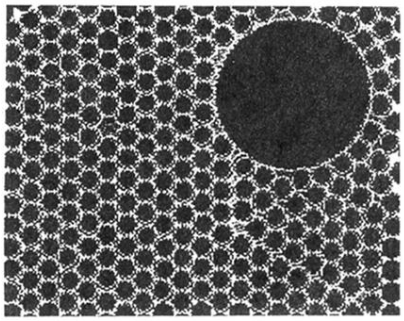

FIG. 2. Bit map showing the detection of particle centers, based on the use of Hough transforms, when two different sizes are present. Circles are drawn around detected particles.